Thermal Stability of Primary S−Nitrosothiols: Roles of Autocatalysis and Structural Effects on the Rate of Nitric Oxide Release

ARTICLE *in* THE JOURNAL OF PHYSICAL CHEMISTRY A · AUGUST 2002

Impact Factor: 2.69 · DOI: 10.1021/jp025756u

4 AUTHORS, INCLUDING:

Silvia Shishido
University of Campinas
13 PUBLICATIONS **285** CITATIONS
SEE PROFILE

Amedea B Seabra
Universidade Federal de São Paulo
80 PUBLICATIONS **1,251** CITATIONS
SEE PROFILE

Nelson Morgon
University of Campinas
76 PUBLICATIONS **758** CITATIONS
SEE PROFILE

Thermal Stability of Primary *S*-Nitrosothiols: Roles of Autocatalysis and Structural Effects on the Rate of Nitric Oxide Release

Marcelo G. de Oliveira,* Sílvia M. Shishido, Amedea B. Seabra, and Nelson H. Morgon

Instituto de Química, Universidade Estadual de Campinas, CP 6154, 13083-970 Campinas, SP, Brazil

Received: March 12, 2002; In Final Form: July 12, 2002

S-Nitrosothiols (RSNOs) are considered to play important roles in storing, transporting, and releasing nitric oxide (nitrogen monoxide, NO) in vivo. Although tertiary RSNOs are known to be intrinsically more stable than primary RSNOs, the correlation between the structure of primary RSNOs and the kinetics of thermal NO release in solution has not been established yet. We have characterized the kinetics of thermal NO release from three primary RSNOs: *S*-nitrosocysteine (CySNO), *S*-nitroso-*N*-acetylcysteine (SNAC), and *S*-nitrosoglutatione (GSNO) in aqueous solutions. It was found that the rates of NO release are strongly affected by the initial concentration of the solutions. Increasing the concentration of CySNO and SNAC from 1.0×10^{-1} to 61.0 mmol L^{-1} led to 5.7- and 14.6-fold increases in their initial rates of decomposition, respectively, whereas GSNO was much less affected (a 2-fold increase). However, a smaller increase in concentration (0.1 to 1.0 mM) led to a 4.6-fold decrease, on average, in the rates of NO release in the three cases. This result was assigned to the combination of an autocatalytic effect promoted by the secondary reaction of thyil radicals with authentic RSNO molecules, which accelerates the decomposition reaction in concentrated solutions, and a nongeminate (diffusive, outside the cage) radical pair recombination effect that leads to a reduction in the rates of reaction in dilute solutions. In the low-concentration range, GSNO and SNAC were shown to be significantly more stable than CySNO. This result is in accordance with the conclusions derived from single-point energy calculations at the MP2/6-31G(2df,p)//MP2/6-31G(d) level of theory, which have shown that the acetamido group that is present in SNAC plays a key role in increasing the S−N bond strength. These results show that comparisons of stability among different *S*-nitrosothiols in solution must take the concentration effect carefully into account and indicate that the half-lives of primary RSNOs found in vivo can be partially determined by their intrinsic structural properties.

Introduction

Since the discovery that mammalian cells produce NO as a short-lived intracellular messenger and its identification as the endothelium-derived relaxing factor (EDRF),[1] interest in the physiological functions of NO has expanded very rapidly. Nitric oxide has been shown to regulate diverse and important processes in biological systems such as smooth-muscle relaxation, magrophage-mediated cytotoxicity, modulation of neurotransmission, regulation of blood pressure, platellet adhesion, and neutrophile aggregation and to be involved in numerous neuronal and nonneuronal functions in the central nervous system and peripheral tissues.[2,3] Because the plasma and cellular milieu contains reactive species that can rapidly inactivate free NO, in contrast to the relatively long half-life of EDRF, it has been considered that NO is stabilized by a carrier molecule that prolongs its half-life and preserves its biological activity. *S*-Nitrosothiols (RSNOs) have been shown to be potent smooth-muscle relaxants and inhibitors of platelet aggregation and are the best candidates for the endogenous storage and transport of NO.[4−10] Some of these compounds such as *S*-nitrosoalbumin (BSNO), *S*-nitroso-L-cysteine (CySNO), and *S*-nitrosoglutatione (GSNO) occur naturally in vivo, and others such as *S*-nitroso-*N*-acetylpenicilamine (SNAP), *S*-nitrosocaptopril, and *S*-nitrosomercaptoethylamine have been synthesized. Their syntheses can be achieved by the *S*-nitrosation reaction of the parent sulfhydryl-containing peptides, which are very reactive toward nitrosating species.[11−13] L-cysteine (CySH) and glutathione (GSH) (the most abundant nonprotein thiol found endogenously) are naturally occurring sulfhydryl-containing peptides found in nearly all cells and have the sulfhydryl group in the cysteine residue. *S*-Nitrosoglutathione (GSNO), formed in the *S*-nitrosation of GSH, has been considered to be an endogenous NO carrier involved in many biological functions.[4,5,12] CySH is the precursor of GSH and has been shown to be involved as an intermediate (*S*-nitrosocysteine, CySNO) in various transnitrosation reactions with other NO carriers.[14,15] *N*-Acetylcysteine (NAC), an endogenous product of cysteine, is also a very effective precursor and stimulator of glutathione synthesis and can be readily nitrosated, yielding *S*-nitroso-*N*-acetylcysteine (SNAC).[16] RSNOs undergo thermal decomposition in solution, yielding free NO and a disulfide according to

$$2\mathrm{RSNO} \rightleftharpoons \mathrm{RS{-}SR} + 2\mathrm{NO} \qquad (1)$$

This reaction is catalyzed by metal ions (especially by Cu^{2+} ions[17]) and is accelerated photochemically by irradiation with ultraviolet or visible light.[16,18,19]

Although the thermal spontaneous release of NO from RSNOs has been reported to be unrelated to the vascular relaxation and antiplatelet properties of these compounds,[20] the correlations between the structure of primary RSNOs and the kinetics of thermal NO release in solution have not been established yet. Most of the current discussion on this subject has been focused

* Corresponding author. E-mail: mgo@iqm.unicamp.br. Phone: +55-0-19-3788-3132. Fax: +55-019-3788-3023.

10.1021/jp025756u CCC: $22.00
Published on Web 08/21/2002

on the observed different stabilities between primary and tertiary *S*-nitrosothiols. Roy et al.[21] have characterized the thermal stability of twelve RSNOs in aqueous solutions and have concluded that the rate of NO release is very sensitive to modifications at the α- and *β*-carbon atoms and also depends on the pH. These dependencies were rationalized in terms of the relative weight of the two resonance structures present in the equilibrium of eq 2.

$$\mathrm{RSN{=}O}_{\text{form I}} \rightleftharpoons \mathrm{RS^{+}{=}NO^{-}}_{\text{form II}} \qquad (2)$$

Any factor favoring form II over form I will lead to an increase in the strength of the S−N bond and will reduce the NO lability. The reason that tertiary RSNOs are more stable than primary RSNOs can thus be interpreted on the basis of an increased electron release from the gem methyl groups, which favors form II. Similarly, the reason that RSNOs are more stable in aqueous acidic solutions can be attributed to a shift of the equilibrium in eq 2 to the right by the protonation of oxygen in $RS^{+}{=}NO^{-}$. Roy et al.[21] have also suggested that the acetamido substituent may stabilize the RSNOs by forming a six-membered cyclic structure where the carbonyl oxygen interacts with the electron-deficient sulfur atom of form II. However, no theoretical calculations were performed to confirm this hypothesis.

Another point of interest in the stability of RSNOs has been the difference in stability between SNAC and *S*-nitroso-*N*-acetylpenicillamine (SNAP). These two RSNOs have similar chemical structures, but whereas SNAC is a primary RSNO, SNAP is a tertiary RSNO with two gem methyl groups at the α-carbon. Bainbrigge et al.[22] have investigated the difference in stability between SNAC and SNAP using DSC/TGA and ab initio calculations on model compounds. Their results indicate that the two gem methyl groups in SNAP do not have a substantial effect on the strength of the S−NO bond and that the enhanced thermal stability may reside in the steric hindrance imposed by the gem methyl groups on the dimerization of the radicals leading to the formation of the sulfur bridge. Although these authors have also analyzed the thermal decomposition of GSNO for a comparison of the strength of the S−NO bond, the great thermal stability of GSNO, which is a primary RSNO, was not interpreted in terms of steric hindrance and remains to be explained. The question of steric interactions affecting the thermal stability of RSNOs was further addressed by Arulsamy et al.,[23] who have contrasted the behavior of Ph_3CSNO and MeSNO with that of GSNO and SNAP. In this study, X-ray diffraction data was used to show that in the solid state, Ph_3CSNO and SNAP have similar bond lengths and angles, with the R−S−N−O linkage adopting a preferable anti conformation. Calculations by density functional theory yielded values of the energy barrier for rotation around the S−N bond that are in agreement with the barrier calculated by variable-temperature ^{15}N NMR. The barrier that was found (44.8 kJ mol^{-1}) indicates that rotation is hindered at room temperature. This is an important conclusion because there is an increase in the S−N bond length at the transition state; consequently, conformational flexibility will influence compound stability. An analysis of the preferable syn or anti conformations was also carried out by Bartberger et al.[24] for primary, secondary, and tertiary *S*-nitrosoalcanothiols. ^{15}N NMR spectra and hybrid density functional calculations have shown that there is an electronic preference for the syn form in CH_3SNO and for the primary and secondary forms in RSNOs, whereas a competing steric effect causes the anti orientation to be favored in the tertiary RSNOs or when the R group is large. A similar conclusion was reached more recently by Lu et al.,[25] who used density functional theory (DFT) to calculate aromatic and aliphatic S−NO bond dissociation energies in the gas phase for two series of thiol-containing model compounds. These authors found that the calculated conformational preference for the C−S−N=O moiety in *S*-nitrosothiophenols and *S*-nitrosobenzylthiol is syn. In another recent study, Grossi et al.[26] monitored the thermal decomposition of three alkylnitrosothiols in *n*-pentane (or *n*-octane) solutions under various reaction conditions. On the basis of kinetic curves fitted to first-order decays and on CG−MS and NMR analyses of the reaction mixtures, these authors claimed that these alkylnitrosothiols undergo thermal decomposition at a rate independent of the bulkiness of the alkyl group and that a possible autocatalytic mechanism involving N_2O_3 as a chain carrier could be operative in aerated solutions.

It can be seen that, despite the recognized biological relevance of RSNOs, the factors that determine their intrinsic stability in solution are still not fully understood. Especially, the great difference in stability found experimentally among primary RSNOs remains, without any satisfactory theoretical explanation. This is partly due to the lack of basic knowledge about how the kinetic behavior of primary RSNOs is related to their structures and conformations, which in turn is a consequence of the difficulties in synthesizing and isolating unstable primary RSNOs. Although the above-mentioned studies furnish important hints to the understanding of the differences in the stabilities of RSNOs relative to the release of NO, they are mainly focused on the properties of alcanothiols (or alkylnitrosothiols) used as model compounds. It is therefore of great importance to know whether this knowledge can be extended to the understanding of the different stabilities of primary RSNOs found endogenously, where the R groups are amino acids or peptides. With this aim, we have used new experimental and theoretical approaches to synthesize three primary RSNOs (CySNO, SNAC, and GSNO) and to establish correlations between the kinetics of thermal NO release and their structures in aqueous solutions.

Experimental Section

Materials. Gaseous NO was obtained from White Martins (Campinas, SP, Brazil). Synthetic air (N_2/O_2, 79/21 v/v, H_2O < 2 ppm, THC, CO + CO_2 < 0.3 ppm) was purchased from Air Liquide (Campinas, SP, Brazil). Anhydrous cysteine (CySH), *N*-acetyl-L-cysteine (NAC), glutathione (GSH), sodium nitrite, and hydrochoric acid were purchased from Aldrich Chemical Co. The above-named reactants were used without further purification. All the experiments were carried out using analytical grade water from a Millipore Milli-Q gradient filtration system. The absence of trace metals in the water, which could catalyze the decomposition of RSNOs, was confirmed by comparing their kinetic curves in the presence and in the absence of DTPA, which showed no significant changes in the rates of decomposition.

RSNOs Synthesis. GSNO was prepared by the reaction of GSH with sodium nitrite in acidic solution, as reported in the literature.[27] GSNO was obtained as stable reddish crystals in the pure form and was dried by freeze drying. CySNO and SNAC cannot be precipitated from solution and stored as solids because of their high solubility in water. For this reason, CySNO and SNAC were synthesized by an alternative method. In this method, a mixture of NO/synthetic air was bubbled through CySH and NAC solutions (61.0 mmol L^{-1}) in a quartz spectrophotometer cuvett. Gas flows were controlled by flowmeters (Aldrich) to obtain mixtures of known NO/air ratios. A gas flow-through system with a glass mixer, polyethylene tubes, and Teflon connections was used to control the mixture and

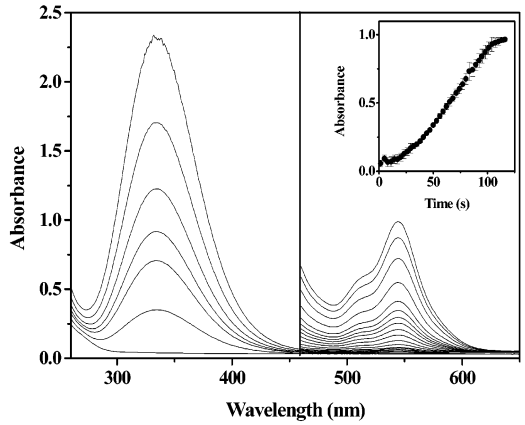

Figure 1. Representative spectral changes in the UV/vis range during the *S*-nitrosation reaction of primary thiols. Formation of SNAC by the *S*-nitrosation of NAC (61.0 mmol L^{-1}) monitored after each gas (NO/air) pulse (For details, see Experimental Section). Spectra were recorded every 3 to 6 s. (Inset) Kinetic curve obtained at 545 nm for the synthesis of SNAC. Error bars correspond to 1 standard deviation (1*s*) of duplicates.

delivery of gases to the solutions. Preadjusted ratios of NO/O_2 (5.6:5.6 mL/min) were used to allow for an excess of O_2 relative to NO. To follow the course of the *S*-nitrosation reaction, the gaseous mixture was bubbled through the solutions in short pulses using a solenoid valve (Cole Parmer) controlled by an electronic circuit developed for this purpose. The reaction was followed spectroscopically at $\lambda = 545$ nm ($\epsilon \approx 34$ M^{-1} cm^{-1}), which corresponds to the maximum of the visible absorption band of the RSNOs. This band and the UV band at 336 nm ($\epsilon \approx 778$ M^{-1} cm^{-1}) were observed to increase continuously over the total bubbling time until a maximum was reached (Figure 1). *S*-Nitrosation was carried out until this maximum was attained to ensure a complete reaction, thus avoiding an excess of the *S*-nitrosating reactant. As a control, this reaction was performed and monitored for four different starting concentrations of CySH and NAC, and the maximum absorbances achieved at the beginning of the plateau (corresponding to the maximum concentrations of RSNO formed) were plotted against the starting RSH concentrations in the range 20−40 mmol L^{-1}. Good linearity was obtained in both cases, indicating that possible parallel reactions do not affect the yield of the main *S*-nitrosation reaction significantly. On the basis of this control, it was assumed that the concentrations of the RSNO solutions that were obtained were equal to the starting concentration of their parent peptide solutions (61.0 mmol L^{-1}). This concentration was used to adjust the absorbance values at 545 nm to 1.0 at the end of the synthesis. Solutions were subsequently diluted to 1.0 mmol L^{-1} and 1.0×10^{-1} mmol L^{-1} in deionized water. This concentration range was used to keep the absorbance values at 336 nm within a suitable range below absorbance 1.0.

For an evaluation of the possible effect of the *S*-nitrosation method on the stability of the RSNOs obtained, SNAC was also synthesized through the reaction of NAC with sodium nitrite in acidic solution as stated above for GSNO. The pH of the freshly prepared RSNOs solutions was measured with an Orion model 410 A pH meter.

Stability of RSNOs Solutions. The stability of RSNO solutions was characterized by monitoring the RSNO concentrations over time, spectrophotometrically. Solutions were placed in quartz cuvetts that were referenced against air, and changes in ground-state absorbances at 25 °C were recorded at 336 nm (for concentrations 1.0×10^{-1} and 1.0 mmol L^{-1}) and at 545 nm (for concentration 61.0 mmol L^{-1}), under stirring, in time intervals of 10 min. These two bands were confirmed to have the same kinetic behavior in the reactions of synthesis and decomposition of the RSNOs. However, the tail of the intense UV band overlaps the weak visible band. For this reason, the UV band was used to monitor the formation and cleavage of the S−N bond in diluted solutions whereas the visible band was used to monitor the decomposition of concentrated solutions. A diode array spectrophotometer (model 8453, Hewlett-Packard, Palo Alto, CA) with a temperature-controlled sample holder was used to monitor the spectral changes. Initial rates of decomposition of the RSNO solutions were obtained by linear regression of the kinetic curves. The absorbance versus time curves at 336 or 545 nm were normalized in order to correct small differences in the starting concentrations of the solutions according to

$$A_N = \frac{A_t - A_i}{A_f - A_i} \tag{3}$$

where A_t, A_i, and A_f are absorbances at times t, initial, and final, respectively, and A_N is the normalized absorbance. Initial rates of decomposition were calculated for all the RSNOs according to

$$I_R = \frac{\Delta A}{\Delta t} \tag{4}$$

where ΔA and Δt are the absorbance change and the corresponding time interval, respectively. Linear regression was done in the initial sections of the kinetic curves, corresponding to extents of reactions of less than 10%.

Theoretical Calculations

All the calculations were performed with the Gaussian[28] and Gammes[29] packages. Full optimizations of molecular geometries and calculations of harmonic vibrational frequencies at the equilibrium geometries were performed at the restricted Hartree−Fock (HF) level by using the Pople 6-31G(d) basis set.[30] These structures were subsequently reoptimized with inclusion of second-order electron correlation effects at the MP2 level, using the same basis set. Final energies were calculated for these geometries at the MP2/6-31G(2df,p)//MP2/6-31G(d) level, considering the 6d and 10f Cartesian functions option and the wave functions of the unperturbed system at the ROHF level.

Results and Discussion

Characterization of the *S*-Nitrosation Reaction. The solutions of RSNOs synthesized by the two methods described above displayed the characteristic absorption bands at 545 and 336 nm (Figure 1). These bands have already been assigned to $n_N \rightarrow \pi^{**}$and $\pi \rightarrow \pi^*$ transitions, respectively,[16,18,19] and were used to confirm the formation of RSNOs in this work. It is known that NO by itself does not react with thiols in solution to yield *S*-nitrosothiols. However, the *S*-nitrosation reaction is observed in aerobic NO solutions.[31,32] In such conditions, the nitrosating species is likely to be N_2O_3, formed according to the following equations:

$$2NO + O_2 \rightarrow NO_2 \tag{5}$$

$$NO + NO_2 \rightleftharpoons N_2O_3 \tag{6}$$

N_2O_3 is a planar molecule with a long $ON-NO_2$ bond (1.864 Å) between the sp^2 nitrogens.[33] Its formation in the gas mixture in equilibrium at room temperature was confirmed by obtaining

the infrared spectrum of the gases (data not shown). N_2O_3 is considered to be the nitrosating species in several *S*-nitrosation reactions,[16,31,32,34,35] although other species such as $OONO^-$ and NO^+ have also been considered to be nitrosating species in other nitrosation reactions.[36] In aqueous solution, N_2O_3 hydrolysis proceeds according to the equilibria

$$N_2O_3 + H_2O \rightleftharpoons 2\,HNO_2 \rightleftharpoons 2NO_2^- + 2H^+ \qquad (7)$$

In this case, the availability of N_2O_3 is highly dependent on the pH. Because the pk_a of nitrous acid[37] is 3.36 and the pHs of aqueous thiol solutions used in the synthesis of RSNOs in this work were in the range 1.4 to 4.0, the equilibrium in eq 8 was driven to the left, providing a source of N_2O_3 for the *S*-nitrosation reaction in all cases. In addition, *S*-nitrosation reactions were not observed above pH 7.0, confirming that hydrolysis of N_2O_3 and *S*-nitrosation act as competing processes. The stoichiometric *S*-nitrosation reaction can thus be written as

$$2N_2O_3 + 3RSH \rightarrow 3RSNO + NO_2^- + H^+ + H_2O \qquad (8)$$

Because the equilibrium of eq 8 is also established in acidic sodium nitrite solutions, reaction 8 can be considered to be the stoichiometric *S*-nitrosation reaction in both nitrosation methods used in this work.

Concentration Effect on the Kinetics of Thermal NO Release from RSNOs. After formation, the three aqueous RSNO solutions showed continuous thermal decomposition in the dark at 25 °C. The thermal NO release was confirmed in each case by following the disappearance of the characteristic absorption bands at 336 and 545 nm assigned to the RSNO group (Figure 1). The disappearance of the bands is concerted with the appearance of a new UV band as a shoulder at ca. 250 nm (not shown), which is consistent with the formation of oxidized RSH, (RS−SR). The formation of dimers shows that the main decomposition pathway is the homolytic cleavage of the S−N bond.

Figure 2 shows the kinetic curves obtained in duplicate experiments of thermal decomposition of the RSNOs over a time range of 3 h. The initial rates of reaction extracted from these curves are presented in Table 1. A control experiment, performed with SNAC, showed that there is no significant difference in the kinetics of decomposition of SNAC synthesized by the two methods described above. This conclusion was extended to the other RSNOs after exactly the same procedures were used in all syntheses.

As can be seen in Figure 2, the kinetic monitoring of the decomposition reactions showed that the initial rates of spontaneous NO release from the three RSNOs in solution are strongly dependent on the starting RSNO concentration. At the concentration 1.0×10^{-1} mmol L^{-1} (curves i), the three RSNOs were shown to be quite stable, with the initial rates of decomposition following the order $I_R(\text{CySNO}) = 1.7 \times I_R(\text{GSNO}) \cong 1.4 \times I_R(\text{SNAC})$. A 10-fold increase in concentration (from 1.0×10^{-1} to 1.0 mmol L^{-1}) led to a further stabilization of the three RSNOs, whose initial rates of decomposition decreased 4.6 times (CySNO), 3.8 times (SNAC), and 5.4 times (GSNO) (curves ii). Under this condition, the initial rates of decomposition follow the order $I_R(\text{CySNO}) = 1.4 \times I_R(\text{GSNO}) \cong I_R(\text{SNAC})$. However, a much greater increase (from 1.0×10^{-1} to 61.0 mmol L^{-1}) in the initial concentration led to an increase in the initial rates of decomposition of CySNO (5.7 times) and SNAC (14.6 times), whereas GSNO was less affected (2-fold increase). Under this condition, the order of initial rates of decomposition obtained was $I_R(\text{SNAC}) = 1.5 \times I_R(\text{CySNO}) = 3.6 \times I_R(\text{GSNO})$. These results show that the relative rates of decomposition of these three primary RSNOs in aqueous solutions (in the absence of other species that might have a catalytic effect) are not governed by their intrinsic stability only. The concentration effect on the rates of decomposition is an indication that diffusion-limited processes must be operative in the homolitic S−N bond cleavage process. This is not surprising, once the radicals RS$^\bullet$ and NO generated in the homolitic bond cleavage of the S−N bond are expected to undergo recombination processes, reforming the reactants. Such processes include geminate and nongeminate recombinations. Geminate recombination corresponds to the reactions of radicals generated from the same precursor molecule and are well-known to be affected by cage effects.[38,39] which are usually expressed by the fluidity dependence of the rates of reaction (or of the quantum yields, in the case of photochemical reactions). We have already reported a cage effect imposed by poly(ethylene glycol) (PEG) matrixes on the thermal and photochemical decomposition of SNAC.[16] In this case, the increased viscosity of PEG leads to an increase in the rate of geminate radical-pair recombination of NAC$^\bullet$ and NO radicals, leading to a decrease in the initial rates of thermal decomposition (and of quantum yields of photochemical decomposition) relative to aqueous solutions. In the present case, the characteristics of the solvent cage are the same under all the conditions analyzed. Thus, geminate recombination is subjected to the same cage effect in all cases. However, the radicals that escape from the solvent cage are subjected to random nongeminate recombination, as a result of encounters during their diffusion through the solution. As a diffusion-limited process, the nongeminate recombination of randomly distributed NO and RS$^\bullet$ radicals is therefore dependent on the concentration of the radical species and thus on the initial RSNO concentrations. The decrease in the rates of decomposi-

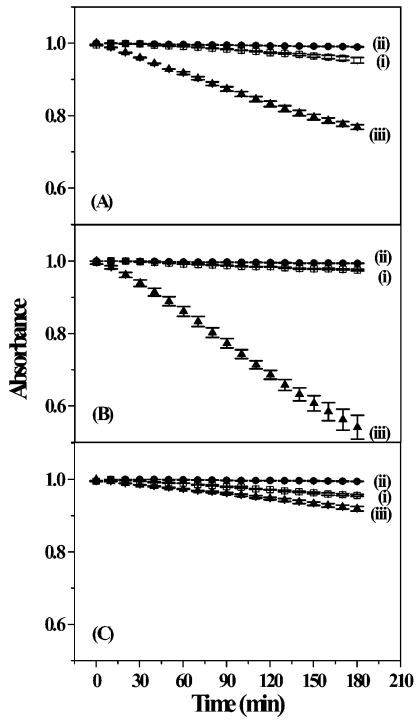

Figure 2. Kinetic curves based on the spectral changes monitored at 336 nm (curves i and ii) and 545 nm (curves iii), corresponding to the thermal NO release from (A) CySNO, (B) SNAC, and (C) GSNO at three different concentrations: 1.0×10^{-1} nmol L^{-1} (i), 1.0 mmol L^{-1} (ii), and 61.0 mmol L^{-1} (iii) at 25° C. Error bars correspond to 1 standard deviation (1*s*) of duplicates.

TABLE 1: Experimental Initial Rates of Reaction for the Thermal Decomposition of Aqueous Unbuffered CySNO, SNAC, and GSNO Solutions at 25 °C in the Dark

	initial rate (s^{-1})		
RSNO (mmol L^{-1})	CySNO	SNAC	GSNO
0.1	$2.6 \times 10^{-4} \pm 6.9 \times 10^{-6}$	$1.6 \times 10^{-4} \pm 3.2 \times 10^{-6}$	$2.1 \times 10^{-4} \pm 7.6 \times 10^{-6}$
1.0	$5.5 \times 10^{-5} \pm 1.2 \times 10^{-6}$	$4.0 \times 10^{-5} \pm 1.0 \times 10^{-6}$	$3.9 \times 10^{-5} \pm 1.1 \times 10^{-6}$
61.0	$1.5 \times 10^{-3} \pm 1.7 \times 10^{-5}$	$2.2 \times 10^{-3} \pm 6.2 \times 10^{-5}$	$4.1 \times 10^{-4} \pm 5.0 \times 10^{-6}$

TABLE 2: Electronic Energies, MP2 and ZPE (au), ΔE, and BDE_{RS-NO} (kJ mol^{-1}) for *S*-Nitrosocysteine (CySNO) and *S*-Nitroso-*N*-acetylcysteine (SNAC) and for the Corresponding Radicals CyS• and NAC• Formed in the Homolitic Cleavage of the S−N Bond with NO Release

species		E_{MP2}	ZPE	E_f[a]	ΔE[b]	BDE_{RS-NO}[c]
NO		−129.652437	0.0051	−129.647883		
CySNO	C1 syn	−849.802300	0.1162	−849.698545	0.00	129.91
	C2	−849.799211	0.1166	−849.695099	9.04	120.29
	C3 anti	−849.799464	0.1165	−849.695441	8.16	126.36
CyS•	RC1	−720.097340	0.1077	−720.001175	0.59	
	RC2	−720.096048	0.1082	−719.999436	5.15	
	RC3	−720.098189	0.1084	−720.001399	0.00	
SNAC	S1 syn	−1002.147851	0.1573	−1002.007397	0.00	152.88
	S2 ts	−1002.067685	0.1561	−1001.928303	207.65	
	S3 anti	−1002.144336	0.1572	−1002.003972	8.99	143.68
	S4	−1002.143523	0.1569	−1002.003427	10.42	118.03
	S5	−1002.138712	0.1568	−1001.998705	22.80	121.92
	S6	−1002.134308	0.1571	−1001.994033	35.10	115.52
NAC•	RS1 syn	−872.434062	0.1487	−872.301288	24.35	
	RS2 anti	−872.442367	0.1476	−872.310575	0.00	

[a] $E_f = E_{MP2} + ZPE(0.893)$. [b] $\Delta E = E_{stable} - E_i$. [c] $BDE_{RS-NO} = E_{RSNO} - (E_{RS} + E_{NO})$.

tion observed when the concentration of RSNOs was increased from 1.0×10^{-1} to 1.0 mmol L^{-1} can thus be assigned to an increase in the rate of random nongeminate radical recombination due to an increase in the frequency of encounters between RS• and NO radicals in the more concentrated solutions.

The great increase in the initial rates of decomposition obtained at 61.0 mmol L^{-1} was rationalized in this work as an autocatalytic effect arising from the reaction between authentic RSNO molecules and RS• radicals formed in the primary decomposition reaction according to

$$RS^{\bullet} + RSNO \rightarrow RS-SR + NO \qquad (9)$$

Reaction 9 also leads to the formation of the thermodynamically stable dimer RS−SR, with the release of another NO molecule. The thyil radical-catalyzed pathway can be expected to be more effective the more concentrated the solution and is reflected in the great increase in the initial rates of decomposition obtained in the 61.0 mmol L^{-1} solutions relative to the lower concentrations used. Although reaction 9 is expected to be operative at all concentrations, the experimental results obtained in this work show that at 61.0 mmol L^{-1} the autocatalytic effect overcomes the cage recombination effect and that the differences are due to the intrinsic stabilities.

It must be noted that at 61.0 mmol L^{-1} the increase in the rate of decomposition of GSNO was much smaller than the increases observed for CySNO and SNAC. This result is probably associated with the much smaller diffusion coefficient that can be expected for the GS• radical, relative to that of radicals CyS• and NAC•, leading to a smaller rate for reaction 9 in the case of GSNO decomposition. It must be noted that whereas reaction 9 involves the diffusion and collision of two bulky species the recombination reaction that regenerates the RSNOs involves the collision between a bulky RS• fragment and a small, fast-diffusing NO molecule. Therefore, it is not surprising that GSNO was the RSNO less affected by the autocatalytic effect.

Geometry Optimizations. Results of the ab initio calculations, including the final electronic energies (E_f) (E_f = EMP2 + ZPE × 0.893) and the energy differences (ΔE) relative to the most stable geometries for CySNO, SNAC, and their corresponding radicals CyS•, NAC•, and NO, together with the bond dissociation energies (BDE) of the RS−NO bond of CySNO and SNAC optimized structures are shown in Table 2. Figure 3 shows the optimized molecular geometries for the energy-minimum structures of CySNO. Only the three most relevant geometries were considered. These geometries encompass the more stable syn and anti conformers defined by the dihedral angle formed by the C−S−N−O group and a less stable syn conformer. Structure C1, corresponding to the syn conformer, was the most stable geometry found. Although the syn conformation also corresponds to the minimum-energy geometry determined theoretically for CH_3SNO,[23,24] there is a fundamental difference between alcanothiols and CySNO. The structure of CySNO (and also those of SNAC and GSNO, see below) allows several types of intramolecular hydrogen bonds involving the −SNO, $-NH_2$, and −COOH groups. The most relevant for analyzing the BDE of the S−N bond are those involving the oxygen and sulfur atoms of the SNO moiety and the hydrogens of the NH_2 and COOH groups, for such hydrogen bonds can lead to an increase in the electronic density between the sulfur and nitrogen atoms and thus to a stabilization effect relative to the release of NO. Structure C1 allows one intramolecular hydrogen bond with a length of 2.905 Å (Hb1) between the oxygen of NO and the hydrogen of the amino group and another with a length of 2.333 Å (Hb2) between the second hydrogen of the amino group and the carbonylic oxygen of the carboxyl group. A second, less stable syn geometry was found (structure C2) that has an intramolecular hydrogen bond between the nitrogen atom of the amino group and the carbonylic oxygen of the carboxyl group (bond length 2.027 Å) (Hb3). Structure C2 has an energy that is 9.04 kJ mol^{-1} above the most stable syn geometry (structure C1). Structure C3 corresponds to the anti conformer. In this structure, Hb1 is absent because of the

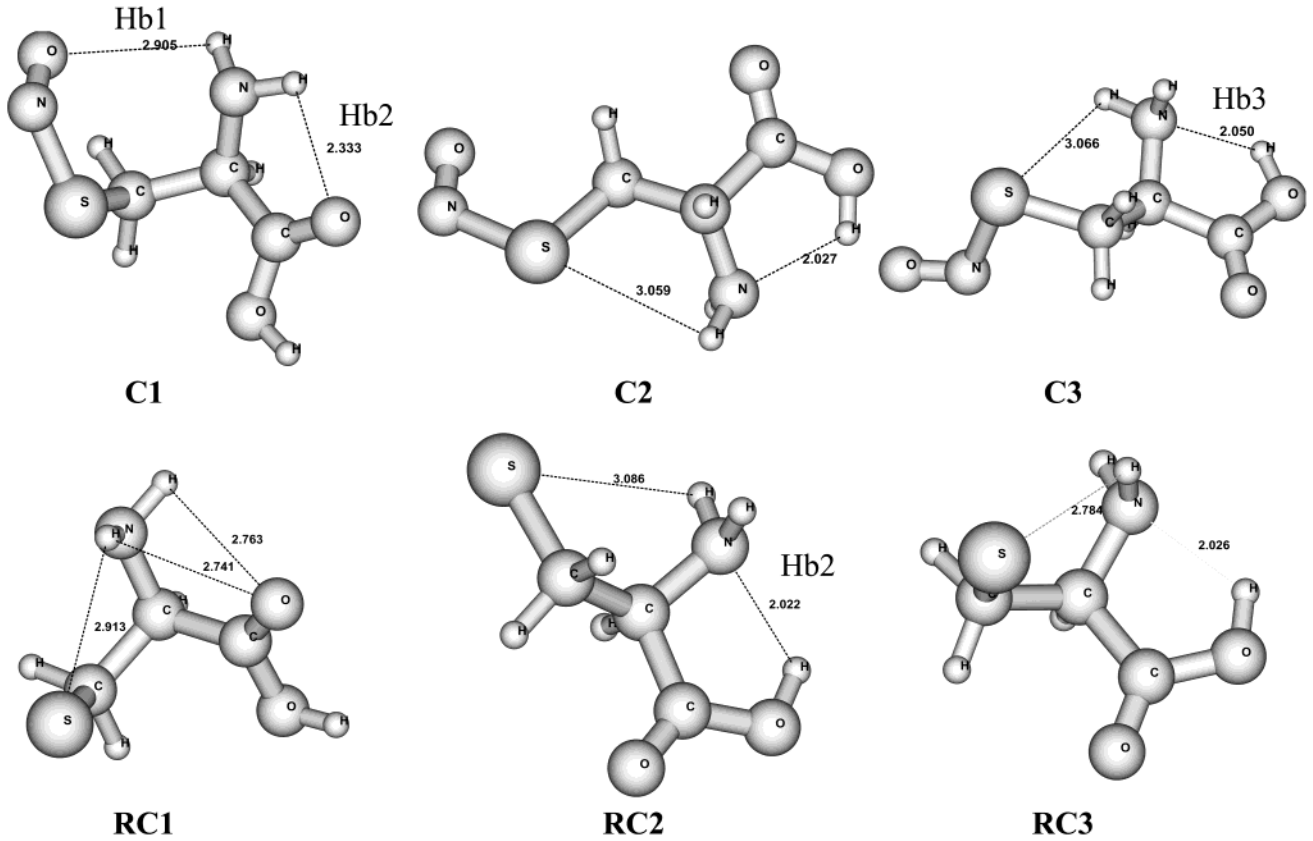

Figure 3. Optimized geometries of CysNO and CyS$^{\bullet}$ at the MP2/6-31G(d) level of theory (distances in Å). (All the optimized geometries are available upon request).

rotation along the C−S axis, which moves the NO moiety far from the amino group.

Structure C3 also allows the interaction Hb3. The highest BDE was found for the syn conformer of structure C1 (129.91 kJ mol^{-1}) (Table 1). It must be noted here that the hydrogen bond Hb2 plays an important role in the orientation of the N−H bond that participates in Hb1.

The almost-planar five-membered ring (−N−H−O−C−C−) that is established in the formation of Hb2 places the axis of the second N−H bond in a position that allows an equilibrium distance of 2.905 Å for the formation of the Hb1 interaction. It can be expected that the Hb1 interaction will place a greater electronic density on the S−N bond, relative to the other structures shown, by favoring form II in the resonance structures of eq 2. As a consequence, there must be an increase in the double bond character, and thus in the BDE of the S−N bond, in structure C1. Such analysis is therefore in accordance with the higher BDE that is found for structure C1. The structures of the radicals resulting from the homolitic bond cleavage of structures C1, C2, and C3 are also shown in Figure 3. It can be seen that the radical resulting from the NO release from C1 (RC1), which is the syn conformer, undergoes a structural rearrangement, allowing a double intramolecular interaction between the hydrogens of the NH_2 group and the carbonylic oxygen of the COOH group. In the radicals resulting from the two other conformers (RC2 and RC3), the strongest hydrogen bond interaction can be expected to occur between the nitrogen of $-NH_2$ and the hydrogen of the −COOH group in RC3, resulting from the cleavage of the anti conformer. Structure RC3 has an energy 0.59 kJ mol^{-1} below the energy of structure RC1.

In the structure of SNAC, one of the hydrogen atoms of the primary amino group is replaced by the acetate group ($-COCH_3$). The carbonylic oxygen of this group can now establish a stronger hydrogen bond with the hydrogen of the carboxylic group attached to the β-carbon of the molecule. This hydrogen bond is indicated as Hb4 in structures S1 and S3 and in the transition structure S2 (ν_i = 755.88 cm^{-1}) in Figure 4 and varies in length from 1.826 to 1.903 Å. In all cases, Hb4 leads to the formation of a seven-membered ring (−H−O−C−C−N−C−O−).

The formation of this ring places the axis of the N−H bond of the amino group at a greater proximity, relative to the oxygen atom of NO in the syn conformer (structures S1 and S2), leading to a stronger hydrogen bond (Hb1) than that formed in the syn conformer of CySNO (structure C1). The strength of this interaction is reflected in its shorter length (2.316 Å) in the syn conformer. Analogous to the stabilization of the S−N bond achieved in the syn conformer of CySNO, the syn conformer of SNAC is also the most stable geometry obtained relative to the BDE of the S−N bond, which in this case is 152.88 kJ mol^{-1} (Table 1).

The syn conformer of SNAC is also 8.99 kJ mol^{-1} more stable than the anti conformer (structure S3), where Hb1 is much longer (3.927 Å). Figure 4 also shows the structure of the transition state in the syn−anti isomerization, characterized by the rotation about the S−N bond (structure S2). The energy barrier obtained for this transition was 207.65 kJ mol^{-1}, which is ca. 4.5 times greater than the values reported in the literature for alcanothiols,[23,24] where Hb1 interaction is absent. This higher energy barrier reflects the energy necessary for the cleavage of Hb1 interaction. Figure 4 shows three additional optimized geometries found for SNAC (structures S4, S5, and S6). It can be seen that the energies of these structures are 10.42 to 35.10 kJ mol^{-1} above the energy of the most stable syn conformer (S1). Only structure S4 allows an intramolecular Hb4 interaction

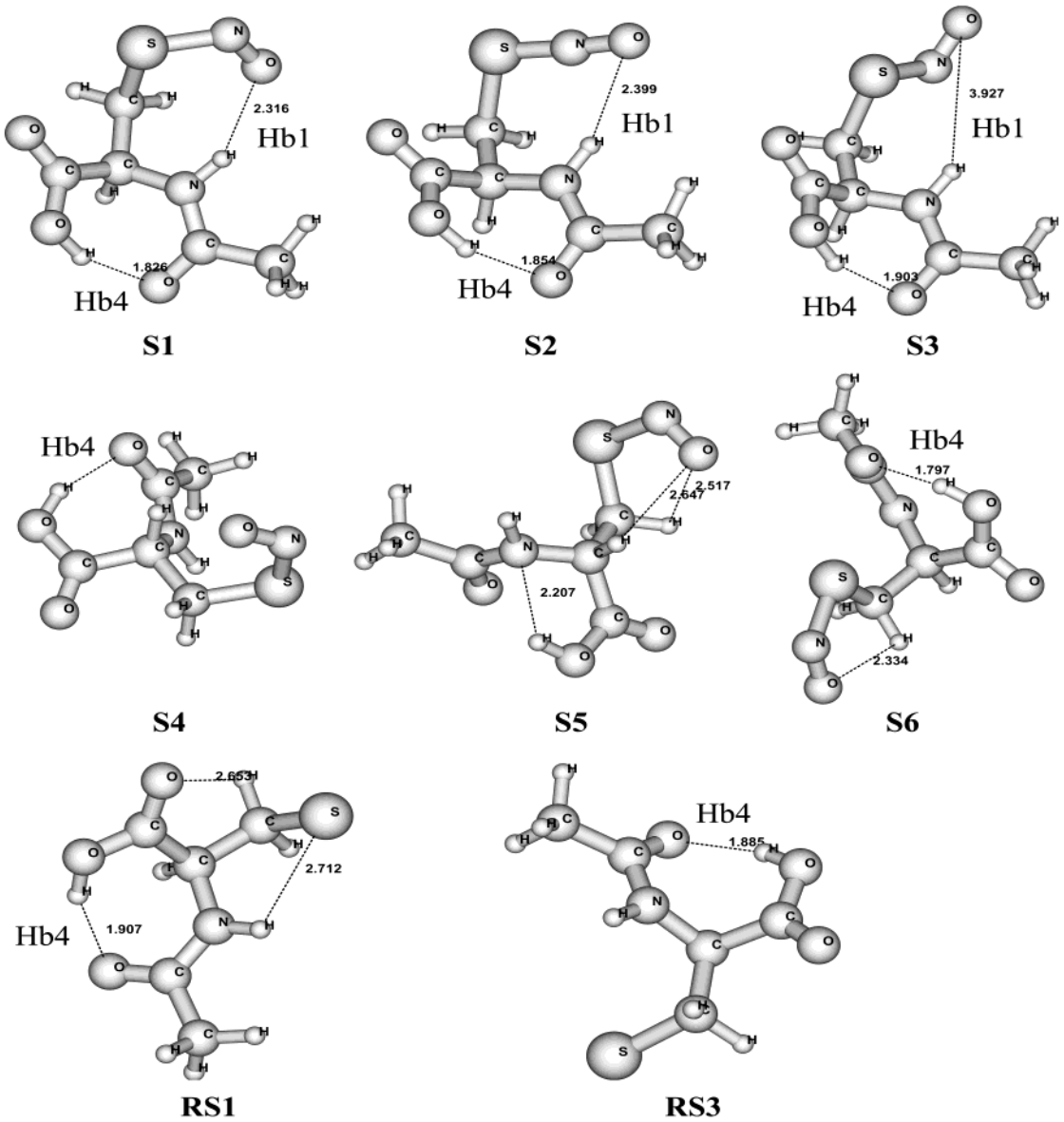

Figure 4. Optimized geometries of SNAC and NAC• at the MP2/6-31G(d) level of theory (distances in Å). (All the optimized geometries are available upon request).

of relevance. Such interaction is probably the cause for the lowest energy found for these three optimized additional geometries. However, the rotation about the C−S bond in S4 moves the NO moiety far from the N−H bond, avoiding the formation of interaction Hb1, which is also absent in the two other geometries presented and in other geometries found but not shown, which have a significantly lower BDE relative to the BDS found for structures S1 and S3 (Table 1). The structures of the radicals resulting from the homolitic bond cleavage of structures S1 and S3 are also shown in Figure 4. It can be seen from the ΔE data of Table 1 that the most stable radical is produced by the release of NO from the anti isomer (RS3). The BDE found for the most stable SNAC geometry (S1) is significantly higher than that found for CySNO (C1). This difference can be understood on the basis of the two stronger and cooperative hydrogen bonds found in SNAC (Hb1 and Hb4) due to the presence of the acetamido group. The reason for the increase in the BDE is thus the same reason claimed in other works (i.e., the favoring of the resonant hybrids with higher electronic density in the S−N bond due to the shift of equilibrium of eq 2 to the right).

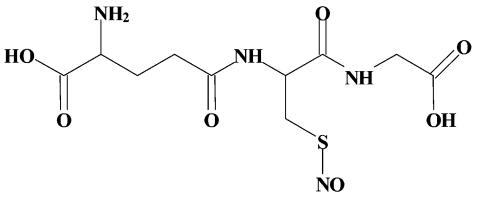

Figure 5. Structure of *S*-nitrosoglutathione (GSNO).

When comparing the relative stability of the three compounds on the basis of their BDE values, it is possible to conclude that SNAC must be more stable than CySNO because of the stabilization effect imposed by the presence of the acetamido group in the former. This conclusion is in accordance with the comparison between the initial rates of decomposition found experimentally for CySNO and SNAC in the concentration range where the autocatalytic effect is minimum.

Because of the time-demanding calculations for the structure of GSNO (Figure 5), theoretical analysis was not included for this molecule in the present work. Further analysis of GSNO, on the basis of ab initio calculations, is currently in progress. GSNO is considered to be a stable NO donor in several works,

while its lower molecular weight analogues CySNO and SNAC are considered to be short-lived NO donors. The experimental data obtained for GSNO in this work shows that its stability is, in fact, very similar to the stability of SNAC in dilute solutions. These results indicate that, similarly to SNAC, GSNO can also be stabilized by intramolecular hydrogen bonds. In addition, its much greater stability in concentrated solution points to the reduced diffusion coefficient of the GS$^{\bullet}$ radical as the cause for the low autocatalytic effect observed, relative to the rates of decomposition of CySNO and SNAC under the same conditions.

Conclusions

It was confirmed that the primary *S*-nitrosothiols CySNO, SNAC, and GSNO release NO spontaneously in aqueous solutions through the homolytic bond cleavage of the S−N bond. The rates of NO release from CySNO, SNAC, and GSNO were found to depend strongly on the initial concentration of the solutions. The acceleration of the decomposition reaction found with the increase in concentration was assigned to an autocatalytic process, arising from the existence of both an uncatalyzed primary unimolecular pathway and a thyil radical-catalyzed pathway, from reactants to products. The decrease in the rate of decomposition observed with the increase in concentration in the range 0.1−1.0 mM was assigned to a nongeminate radical-pair recombination effect, which leads to a reduction in the rate of reaction due to the increase in the rate of recombination between radicals NO and RS$^{\bullet}$. Although present in all concentrations, the autocatalytic effect overcomes the recombination effect in more concentrated solutions. This result shows comparisons of stability among different *S*-nitrosothiols in solution and must take the concentration effect carefully into account. In the low-concentration range, GSNO and SNAC were shown to be significantly more stable than CySNO. The experimental results for CySNO and SNAC are in accordance with the conclusions derived from single-point energy calculations at the MP2/6-31G(2df,p)//MP2/6-31G(d) level of theory, which have shown that the acetamido group, present in SNAC, plays a key role in increasing the S−N bond strength and thus in decreasing the NO lability. These results indicate that for low-concentration ranges, where primary RSNOs are found in vivo, their half-lives in reactions of transfer and release of NO can be partially determined by their intrinsic structural properties.

Acknowledgment. S.M.S. and A.B.S hold graduate fellowships from Fundação de Amparo à Pesquisa do Estado de São Paulo (FAPESP), grant numbers 98/03738-9 and 01/7869-9, respectively. We thank FAPESP and CNPq for financial support.

References and Notes

(1) Ignarro, L. J.; Buga, G. M.; Wood, K. S.; Byrns, R. E.; Chaudhuri, G. *Proc. Natl. Acad. Sci. U.S.A.* **1987**, *84*, 9265.

(2) Lancaster, J., Jr. *Nitric Oxide: Principles and Actions*; Academic Press: San Diego, CA, 1996; p 1.

(3) Stamler, J. S.; Singel, D. J.; Loscalzo J. *Science (Washington, D.C.)* **1992**, *258*, 1898.

(4) Askew, S. C.; Butler, A. R.; Flitney, F. W.; Kemp, G. D.; Megson, I. L. *Bioorg. Med. Chem.* **1995**, *3*, 1.

(5) Clancy, R. M.; Levartovsky, D.; Leszczynska-Piziak, J.; Yegudin, J.; Abranson, S. B. *Proc. Natl. Acad. Sci U.S.A.* **1994**, *91*, 3680.

(6) Mathews, W. R.; Kerr, S. Q. *J. Pharmacol. Exp. Ther.* **1993**, *267*, 1529.

(7) Garbor, G.; Allon, N.; Weetall, H. H. *Microchem. J.* **1997**, *56*, 177.

(8) Kaye, D. M.; Wiviott, S. D.; Kobzik, L.; Kelly, R. A.; Smith, T. W. *Am. J. Physiol.* **1997**, *272*, H875.

(9) Hoog, N. *Free Radical Biol. Med.* **2000**, *28*, 1478.

(10) Szacilowski, K.; Stasicka, Z. *Prog. React. Kinet. Mech.* **2000**, *26*, 1.

(11) Stamler, J. S.; Simon, D. I.; Osborne, J. A.; Mullins, M. E.; Jaraki, O.; Michel, T.; Singel, D. J.; Loscalzo, J. *Proc. Natl. Acad. Sci. U.S.A.* **1992**, *89*, 444.

(12) Wink, D. A.; Nims, R. W.; Darbyshire, J. F.; Christodoulou, D.; Hanbauer, I.; Cox, G. W.; Laval, F.; Laval, J.; Cook, J. A.; Krishna, M. C.; DeGraff, W. G.; Mitchell, J. B. *Chem. Res. Toxicol.* **1994**, *7*, 519.

(13) Jocelyn, P. C. *Biochemistry of the SH Group*; Academic Press: London, 1972; p 240.

(14) Liu, Z. G.; Rudd, M. A.; Freedman, J. E.; Loscalzo, J. *J. Pharmacol. Exp. Ther.* **1998**, *284*, 526.

(15) Park, J. W.; Billman, G. E.; Means, G. E. *Biochem. Mol. Biol. Int.* **1993**, *30*, 885.

(16) Shishido, S. M.; de Oliveira, M. G. *Photochem. Photobiol.* **2000**, *71*, 273.

(17) Williams R. J. P. *Chem. Soc. Rev.* **1996**, 77.

(18) Sexton, D. J.; Muruganandam, A.; McKenney, S. J.; Mutus, B. *Photochem. Photobiol.* **1994**, *59*, 463.

(19) Wood, P. D.; Mutus, B.; Redmond, R. W. *Photochem. Photobiol.* **1996**, *64*, 518.

(20) Kowaluk, E. A.; Fung, H. L. *J. Pharmacol. Exp. Ther.* **1990**, *255*, 1256.

(21) Roy, B.; d'Hardemare, A. M.; Fontecave, M. J. *Org. Chem.* **1994**, *59*, 7019.

(22) Bainbrigge, N.; Butler, A. R.; Gorbitz, C. H. *J. Chem. Soc., Perkin Trans. 2* **1997**, *2*, 351.

(23) Arulsamy, N.; Bohle, D. S.; Butt, J. A.; Irvine, G. J.; Jordan, P. A.; Sagan, E. *J. Am. Chem. Soc.* **1999**, *121*, 7115.

(24) Bartberger, M. D.; Houk, K. N.; Powell, S. C.; Mannion, J. D.; Lo, K. Y.; Stamler, J. S.; Toone, E. *J. Am. Chem. Soc.* **2000**, *122*, 5889.

(25) Lu, J. M.; Wittbrodt, J. M.; Wang, K.; Wen, Z.; Shlegel, H. B.; Wang, P. G.; Cheng, J. P. *J. Am. Chem. Soc.* **2001**, *123*, 2903.

(26) Grossi, L.; Montevecchi, P. C.; Strazzari, S. *J. Am. Chem. Soc.* **2001**, *123*, 4853.

(27) Hart, T. W. *Tetrahedron Lett.* **1985**, *26*, 2013.

(28) Frisch, M. J.; Trucks, G. W.; Schlegel, H. B.; Scuseria, G. E.; Robb, M. A.; Cheeseman, J. R.; Zakrzewski, V. G.; Montgomery, J. A., Jr.; Stratmann, R. E.; Burant, J. C.; Dapprich, S.; Millam, J. M.; Daniels, A. D.; Kudin, K. N.; Strain, M. C.; Farkas, O.; Tomasi, J.; Barone, V.; Cossi, M.; Cammi, R.; Mennucci, B.; Pomelli, C.; Adamo, C.; Clifford, S.; Ochterski, J.; Petersson, G. A.; Ayala, P. Y.; Cui, Q.; Morokuma, K.; Malick, D. K.; Rabuck, A. D.; Raghavachari, K.; Foresman, J. B.; Cioslowski, J.; Ortiz, J. V.; Stefanov, B. B.; Liu, G.; Liashenko, A.; Piskorz, P.; Komaromi, I.; Gomperts, R.; Martin, R. L.; Fox, D. J.; Keith, T.; Al-Laham, M. A.; Peng, C. Y.; Nanayakkara, A.; Gonzalez, C.; Challacombe, M.; Gill, P. M. W.; Johnson, B. G.; Chen, W.; Wong, M. W.; Andres, J. L.; Head-Gordon, M.; Replogle, E. S.; Pople, J. A. *Gaussian 98*, revision A.7; Gaussian, Inc.: Pittsburgh, PA, 1998.

(29) Schmidt, M. W.; Baldridge, K. K.; Boatz, J. A.; Elbert, S. T.; Gordon, M. S.; Jensen, J. H.; Koseki, S.; Matsunaga, N.; Nguyen, K. A.; Su, S. J.; Windus, T. L.; Dupuis, M.; Montgomery, J. A. *J. Comput. Chem.* **1993**, *14*, 1347.

(30) Hehre, W. J.; Ditchfield, R.; Pople, J. A. *J. Chem. Phys.* **1972**, *56*, 2257.

(31) Wink, D. A.; Nims, R. W.; Darbyshire, J. F.; Christodoulou, D.; Hanbauer, I.; Cox, G. W.; Laval, F.; Laval, J.; Cook, J. A.; Krishna, M. C.; DeGraff, W. G.; Mitchell, J. B. *Chem. Res. Toxicol.* **1994**, *7*, 519−525.

(32) Kharitnov, V. G.; Sundauist, A. R.; Sharma, V. S. *J. Biol. Chem.* **1995**, *270*, 28158−28164.

(33) Simon, A.; Horakh, J.; Obermeyer, A.; Borrmann, H. *Angew Chem., Int. Ed. Engl.* **1992**, *31*, 301−303.

(34) Stamler, J. S.; Simon, D. I.; Osborne, J. A.; Mullins, M. E.; Jaraki, O.; Michel, T.; Singel, D. J.; Loscalzo, J. *Proc. Natl. Acad. Sci. U.S.A.* **1992**, *89*, 444.

(35) Gow, A. J.; Buerk, D. G.; Ischiropoulos, H. *J. Biol. Chem.* **1997**, *272*, 2841.

(36) Wink, D. A.; Darbyshire, J. F.; Nims, R. N.; Saavedra, J. E.; Ford, P. C. *Chem. Res. Toxicol.* **1993**, *6*, 23.

(37) Fasman, G. D. *CRC Handbook of Biochemistry and Molecular Biology*, 3rd ed.; CRC Press: Boca Raton, FL, 1985; Vol. 1, p 224.

(38) Wayne, R. P. *Principles and Applications of Photochemistry*; Oxford Science Publications: Oxford, U.K., 1991; p 54.

(39) Stochel, G. *Coord. Chem. Rev.* **1992**, *114*, 269.